



**Mechanical Performance and Machinability of Hybrid
FRP Composite Via Abrasive Water-Jet Machining
using Response Surface Methodology and Numerical
Model**

by

**IRINA WONG MING MING
(1540511678)**

A thesis submitted in fulfillment of the requirements for the degree of
Doctor of Philosophy

**School of Manufacturing Engineering
UNIVERSITI MALAYSIA PERLIS**

2019

DEDICATION

To:

My Dearest Parents,

Mr. Wong King Hock & Mrs. Lau Wu Hee

My Handsomest Eldest Brother and Lovely Sister in Law and Niece,

Wong Kiing Aik, Lau Lu Fei and Yilia Wong

My Pretties Sister and Handsome Brother in Law

Winnie Wong and Chieng Leh Yong

My Handsomest Younger Brothers,

Wong Kiing Seng and Wong Kiing Ing

ACKNOWLEDGEMENTS

First and foremost, I would like to express my sincerest gratitude to my supervisor, Dr. Azwan Iskandar Bin Azmi for his unreserved guidance, constructive suggestions, through inspiring discussion and continuous encouragement throughout this doctoral study. I appreciate all his patient guidance, contributions of time and ideas that assisted me in completing my PhD study. I am also thankful to my co-supervisor, Dr. Lee Chang Chuan and Dr Ahmad Humaizi Bin Hilmi for their guidance and constant support during this work. The completion of this project would not be achieved without their assistance and guidance.

In addition, I am grateful acknowledge receiving helpful assistance from the engineer staff of KTPC, Kulim Hi-tech Park for their unending technical support in operating abrasive waterjet machine. Their valuable suggestions and discussions enabled me to overcome the issues arose during work. My appreciation is also expressed to thank all of the staffs in UniMAP for fruitful collaboration and friendly working atmosphere. Special thanks to Dr. Tan Chye Lih, En. Suhelmi, En. Mazlan, En. Mohd. Nazri and En. Mohd. Jasmin. Thanks for their help, knowledge and skills as well as the mentally support that I have gained from them, really appreciate it. Furthermore, I would like to thank my friend from Manufacturing postgraduate group and all the friendly lecturers for their useful opinions and motivation over the duration of this doctoral study.

And most importantly, I would like to express my deepest appreciation for my parents and siblings, for their unconditional love and encouragements that has given me to overcome many challenges and eventually complete thesis. They were willing to support any decision I made, although it was hard for them to understand my study and difficulties. My parents have been unsurpassed at all times, and from this, I am eternally indebted. Baba and Mammy, I love you now and forever. Thank you for loving me.

TABLE OF CONTENTS

	PAGE
THESIS DECLARATION	Ii
DEDICATION	Iii
ACKNOWLEDGEMENTS	Iv
TABLE OF CONTENTS	V
LIST OF TABLES	Xi
LIST OF FIGURES	Xiii
LIST OF ABBREVIATIONS	Xvii
	i
LIST OF SYMBOLS	Xx
ABSTRAK	Xxii
ABSTRACT	Xxii
	i
CHAPTER 1: INTRODUCTION	1
1.1 Background	1
1.2 Problem Statement	3
1.3 Research Objectives	4
1.4 Significance of Study	5
1.5 Thesis Outline	6
CHAPTER 2: LITERATURE REVIEW	8

2.1	Background	8
2.2	Fibre-Reinforced Polymer (FRP) Composite Material	8
2.3	Machining of FRP Composite	18
2.3.1	Overview of Abrasive Water-Jet Machining	21
2.3.2	Principle of Abrasive Water-jet Machining (AWJM)	23
2.4	Material Removal Process of AWJM	26
2.4.1	Micro-mechanism of AWJM	27
2.4.2	Macro-mechanism of AWJM	29
2.5	Parameter Study for Abrasive Water-jet Cutting	31
2.5.1	Influence of Hydraulic Pressure Process Parameters	32
2.5.2	Influence of Geometric Process Parameters	33
2.5.3	Influence of Abrasive Properties Process Parameters	34
2.5.4	Influence of Cutting Process Process Parameters	36
2.5.5	Summary	38
2.6	AWJM Process Modeling and Simulation	39
2.7	Identified Gaps in the Literature	43
2.7.1	Influence of Hydraulic Pressure Process Parameters	43
2.7.2	Influence of Hydraulic Pressure Process Parameters	45
2.7.2.1	Fibre-Dominated Failure Modes	46
2.7.2.2	Matrix-Dominated Damage	51
2.8	Identified Gaps in the Literature	55

CHAPTER 3: EXPERIMENTAL METHODOLOGY	57
3.1 Introduction	57
3.2 Phase 1: Characterization of Hybrid FRP Composites	59
3.2.1 Selection of Fibre Reinforcement and Polymer Matrix	59
3.2.2 Manufacturing and Fabrication Procedure of Composite Panels	60
3.2.3 Mechanical Testing of Hybrid FRP composites	63
3.2.4 Scanning Electron Microscopy (SEM)	66
3.3 Phase 2: Machinability Performance of the Hybrid FRP Composite using AWJM	67
3.3.1 Design of Experiment (DOE)	67
3.3.2 Selection of Machinability Parameters	69
3.3.2.1 Stage 1: 2 ⁴ Factorial Design	71
3.3.2.2 Stage 2: RSM Face-centred Central Composite Design (FCD)	72
3.3.3 AWJM and Experimental Setup	74
3.3.4 Data Acquisition Equipment and Procedure	76
3.3.4.1 Kerf Ratio Measurement	76
3.3.4.2 Surface Roughness Measurement	78
3.3.4.3 Delamination damage and factor	80
3.3.5 ANOVA and Confirmation Test	82
3.4 Model Implementation	84

3.4.1	Model Assumption and Limitations	85
3.4.2	Finite Element Model	87
3.4.3	Deletion of Elements with Physical Distortion	88
3.5	Summary	89
CHAPTER 4: MECHANICAL PROPERTIES OF HYBRID FRP COMPOSITES OF DIFFERENT ARCHITECTURES		89
4.1	Introduction	89
4.2	Fibre Volume Fractions and Densities	91
4.3	Tensile Strength of Hybrid FRP Composites	96
4.4	Flexural Strength of Hybrid FRP Composites	102
4.5	Summary	107
CHAPTER 5: EXPERIMENTAL RESULTS ON ABRASIVE WATER-JET MACHINING		109
5.1	Introduction	109
5.2	Overall Experimental Results	110
5.2.1	Experimental Results on Kerf Ratio, T_R	110
5.2.1.1	Statistical Analysis on the Effect of AWJM Parameters on Kerf Ratio, T_R	112
5.2.1.2	Empirical model using RSM for Kerf Ratio, T_R	113
5.2.1.3	Discussion on the Effect of AWJM Parameters towards Kerf Ratio, T_R	115
5.2.2	Experimental Results on Delamination Damage, F_d	120

5.2.2.1	Statistical Analysis on the Effect of AWJM Parameters on Delamination Damage and Factor	123
5.2.2.2	Empirical model using RSM for Delamination Factor, F_d	125
5.2.2.3	Discussion on the Effect of AWJM Parameters towards Delamination Damage and Factor	128
5.2.3	Experimental Results on Surface Roughness, R_a	137
5.2.3.1	Statistical Analysis on the Effect of AWJM Parameters on Surface Roughness, R_a	143
5.2.3.2	Empirical model using RSM for Surface Roughness, R_a	145
5.2.3.3	Discussion on the Effect of AWJM Parameters towards Surface Roughness, R_a	147
5.3	Optimisation of Trimming Condition for Hybrid FRP Composites	154
5.4	Summary	157
	CHAPTER 6: NUMERICAL STUDY ON THE DAMAGE RESPONSE OF COMPOSITE LAMINATES AFTER ABRASIVE WATER-JET CUTTING/PIERCING IN ABAQUS	158
6.1	Overview of Damage Model	158
6.2	Results and Discussion	159
6.2.1	Qualitative and Quantitative Results of AWJ Simulation	160
6.2.2	Meso-mechanism of AWJM for Hybrid FRP Composites through Simulation Modelling	164
6.3	Summary	168
	CHAPTER 7: CONCLUSIONS AND RECOMMENDATIONS FOR FUTURE WORKS	169

7.1 Conclusion	169
7.2 Recommendation for Future Works	171
REFERENCES	173
LIST OF PUBLICATIONS	183
APPENDIXS	188

©This item is protected by original copyright

LIST OF TABLES

		PAGE
Table 2.1	Applications of polymer matrix composite (Matthews & Rawlings, 1999; Sheikh-Ahmad, 2009)	10
Table 2.2	Typical properties of reinforcing fibres (Kalpakjian & R. Schmid, 2010; Sheikh-Ahmad, 2009)	15
Table 3.1	Specifications of fibre reinforcements	60
Table 3.2	Process parameters and the levels used in RSM	70
Table 3.3	A 2^k factorial design of experiments (2^4) with centre points	72
Table 3.4	Augmented design of experiments for RSM	73
Table 3.5	Details of the constant parameters for the AWJM	76
Table 3.6	Surface roughness measurement condition per region	80
Table 3.7	Material properties of the weaved glass fibre laminates and weaved carbon fibre laminates	86
Table 4.1	Physical properties of hybrid fibre reinforcement polymer composite	92
Table 4.2	Tensile properties of hybrid FRP composites	97
Table 4.3	Failure of hybrid composite laminates under tensile load	98
Table 4.4	Flexural properties of hybrid fibre reinforced polymer composites	103
Table 4.5	View of failed hybrid composite laminates under flexural loading	106
Table 5.1	Experimental results for kerf ratio, T_R based on 24 orthogonal arrays	111
Table 5.2	ANOVA analysis for T_R (after backward elimination with p-value < 0.05)	113
Table 5.3	Augmented design of experiment for kerf ratio, T_R	114

Table 5.4	ANOVA for the T_R quadratic polynomial model	115
Table 5.5	Experimental results for delamination factor (damage), F_d based on a 2^4 orthogonal array	121
Table 5.6	ANOVA analysis for $F_{d(entrance)}$ (after backward elimination)	124
Table 5.7	ANOVA analysis for $F_{d(exit)}$ (after backward elimination)	124
Table 5.8	Augmented design of experiment for delamination damage, F_d	125
Table 5.9	ANOVA for the $F_{d(entrance)}$ quadratic polynomial model	126
Table 5.10	ANOVA for the $F_{d(exit)}$ two-interaction model	127
Table 5.11	Results for surface roughness based on a 2^4 orthogonal array	140
Table 5.12	ANOVA analysis for R_a (after backward elimination with P-value <0.05)	144
Table 5.13	Augmented design of experiment for surface roughness, R_a	145
Table 5.14	ANOVA for the R_a using quadratic polynomial model	146
Table 5.15	Constraints for optimisation of the AWJM process	155
Table 5.16	Results of optimisation	156
Table 5.17	Comparison of predicted value and actual validation run	156
Table 5.18	Point prediction at 95% prediction interval (PI)	156
Table 5.19	Effect of processing parameters on process responses in AWJM	156

LIST OF FIGURES

	PAGE
Figure 1.1 Hybrid composite configurations: (a) interplay, (b) intraply, and (c) intimately mixed (Swolfs et al., 2014)	1
Figure 2.1 Notation of (a) unidirectional fibre (Gay, Hoa, & Tsai, 2003) (b) weaved fibre (Chittajallu, 2004) and (c) bi-axial $\pm 45^\circ$ fibre (Mazumdar, 2002)	12
Figure 2.2 Mechanical properties of FRP composites with differing loading direction (Taranu et al., 2008)	13
Figure 2.3 Common machining processes for FRP composites (Nedelcu, Mihai, & Giboin, 2013)	19
Figure 2.4 Typical in plane damage of FRP composites (Mallick, 2007)	20
Figure 2.5 Various modes of delamination (Kormaniková & Kotrasová, 2017)	20
Figure 2.6 Abrasive feed system and cutting head assembly (Pahuja, 2015)	23
Figure 2.7 Schematic of AWJM system (Anwar, 2013)	24
Figure 2.8 General structure of cutting head system for AWJM (Alsoufi, 2017)	24
Figure 2.9 Sub-mechanisms of erosion mechanisms (Meng & Ludema, 1995)	27
Figure 2.10 Micro-mechanism of machining ductile material	28
Figure 2.11 Failure modes for brittle materials (Gajera & Swarrop, 2014; Jankovic et al., 2013)	28
Figure 2.12 Surface generated of aluminium alloy through abrasive water-jet cutting (Jankovic et al., 2013)	29
Figure 2.13 Image of micrograph of an AWJM GFRP laminate (Ramulu & Arola, 1994)	30
Figure 2.14 Formation of distinct regions in abrasive water-jet cutting (Anwar, 2013)	31
Figure 2.15 Process parameter that affecting abrasive water-jet performance (Ramulu, Pahuja, Hashish, & Isvilonanda, 2015)	32

Figure 2.16	Increasing jet divergence with stand-off distance (Srinivasu et al., 2009)	37
Figure 2.17	AWJM process modelling and simulation in different districts	40
Figure 2.18	Structure of high velocity water-jet in air (Guha et al., 2010)	41
Figure 2.19	Particle approximations using particles within the influence domain of the smoothing function W for Particle A.	44
Figure 2.20	Failure modes in weaved fibre reinforced composite laminates (Liu et al., 2018)	46
Figure 2.21	Fibre-dominated damage with associated fracture plane (Chiu, 2015)	46
Figure 2.22	Bilinear stress-strain law (Chiu, 2015)	47
Figure 2.23	Stress-strain response during fibre direction loading/unloading: path 1-2, tensile load; path 3, unload; path 4-5, load in compression; path 6-8, compressive unload and tensile reload until failure. (Chiu, 2015)	50
Figure 2.24	Matrix-dominated fracture with associated fracture plane (Chiu, 2015)	52
Figure 2.25	Coordinate system attached to the fracture plane (1,N,T) relative to the material coordinate system (1,2,3). (Chiu et al., 2015)	52
Figure 3.1	Flow of research work in this doctoral study	58
Figure 3.2	Close-up views of the fibre reinforcements: (a) plain weaved carbon fibres; (b) plain weaved E-glass plain fibres; (c) stitched biaxial ($\pm 45^\circ$) E-glass fibres.	59
Figure 3.3	Schematic of VARTM process (Azmi, 2012)	61
Figure 3.4	Complete setup of VARTM	62
Figure 3.5	Burn-off test using Nabertherm furnace	63
Figure 3.6	The universal testing machine used for tensile and flexural tests	65
Figure 3.7	Three-point bending or flexural test	65
Figure 3.8	Hitachi TM3000 scanning electron microscope with EDX capability	67
Figure 3.9	Flow of DOE to obtain an optimal model	68
Figure 3.10	Ishikawa cause and effect diagram or fish bone diagram for the AWJM process (Gaidhani, 2013; Kechagias et al., 2012)	69

Figure 3.11	Four-factor cube plot (red dots = centre point)	71
Figure 3.12	Face-centred central composite design	73
Figure 3.13	Experimental setup of the abrasive water-jet cutting machine	75
Figure 3.14	Specimen design (red box = kerf slot)	77
Figure 3.15	Kerf geometry of a through-cut composite trimmed by the AWJM (Arola & Ramulu, 1996)	77
Figure 3.16	Mitutoyo Crystal-Plus M574 coordinate measuring machine equipped with Renishaw A-5000-7800 ruby ball stylus	78
Figure 3.17	Mitutoyo CS-3000 525-780E-1 surface roughness tester	78
Figure 3.18	Surface region for measuring surface roughness	79
Figure 3.19	Topper XDC-10 zoom lense microscope	81
Figure 3.20	Delamination damage measurement	81
Figure 3.21	Flow diagram of mesoscopic computation of hybrid FRP composite through AWJM	83
Figure 3.22	FE model for a hybrid composite plate with abrasive water-jet tube, (a) full view, close-up of (b) abrasive water-jet and (c) hybrid composite plate.	85
Figure 4.1	Stacking configurations of carbon fibre (C), E-glass plain weaved (W) and E-glass stitch bi-axial $\pm 45^\circ$ (B) fibre plies in FRP laminates	91
Figure 4.2	Hybrid FRP composite specimen before and after the burn-off test	92
Figure 4.3	Comparison of fibre volume fraction with others fabrication method (Pandya et al., 2011; Zhang et al., 2012a; Tan et al., 2016)	94
Figure 4.4	Comparison of density of hybrid composites with different architecture of fibre	95
Figure 4.5	Failure mode of hybrid composite under the tensile test: (a) [BC] ₆ , (b) [CBBC] ₃ , and (c) [CW ₂] ₆	97
Figure 4.6	Stress-strain curve for different laminate orientations of the hybrid FRP composites	101
Figure 4.7	Comparisons of tensile responses for different orientations of hybrid and monolithic FRP composites	101

Figure 4.8	Flexural test sample is completely bends after flexural loading or complete bending of test sample after flexural test	102
Figure 4.9	Flexural stress-strain curve for different laminate orientations of FRP composites	105
Figure 5.1	Cross-section of hybrid carbon/glass composites with abrasive water-jet cutting: (a) Experiment 1 (SOD: 2 mm), (b) Experiment 5 (SOD: 5 mm), and (c) Experiment 2 (SOD: 8 mm)	116
Figure 5.2	Main effect plots of the top and bottom kerf widths for (a) abrasive flow rate, (b) hydraulic pressure, (c) SOD and (c) traverse rate	116
Figure 5.3	Perturbation plot showing the effect of stand-off distance and traverse rate on kerf ratio, T_R	119
Figure 5.4	Delamination factor change in the entrance and exit jets	121
Figure 5.5	Mechanism of delamination: (a) fracture initiation and (b) water-jet induced delamination at exit	122
Figure 5.6	Main effect plots of delamination factor for (a) abrasive flow rate, (b) hydraulic pressure, (c) SOD and (d) traverse rate	128
Figure 5.7	Cutting front with an abrasive water-jet at high traverse speeds	131
Figure 5.8	Response surface and contour plots for interaction on $F_{d(entrance)}$ [abrasive flow rate = 360 g/min & hydraulic pressure = 2600 mm/min	132
Figure 5.9	Response surface and contour plot interaction on $F_{d(exit)}$ when other variables are at a constant level: (a) abrasive flow rate and hydraulic pressure; (b) abrasive flow rate and traverse rate; (c) hydraulic pressure and traverse rate	133
Figure 5.10	Perturbation plot showing the effect of all factors on (a) $F_{d(entrance)}$ and (b) $F_{d(exit)}$	134
Figure 5.11	Mechanism of delamination versus stand-off distance (a) 2 mm, (b) 5 mm and (c) 8 mm	136
Figure 5.12	A comparison of surface roughness at the top, middle, and bottom of trimmed wall surface	138
Figure 5.13	Cross-section surface for Experiment 16 and Experiment 13	140
Figure 5.14	SEM images of an AWJM surface for Experiment 13	141
Figure 5.15	SEM image of cross-section surface of (a) Experiment 16 and (b) Experiment 13	142

Figure 5.16	Main effect plots for surface roughness	148
Figure 5.17	Cross-section surface for Experiment 13	149
Figure 5.18	Jet divergence after exiting from the abrasive water-jet focusing nozzle	150
Figure 5.19	Response surface and contour plots that represent the effect of two variables and their interaction on R_a when the other variables are at a middle level for: (a) abrasive flow rate and hydraulic pressure; (b) abrasive flow rate and traverse rate; (c) hydraulic pressure and traverse rate	152
Figure 5.20	Perturbation plot showing the effect of all factors on R_a	153
Figure 6.1	Damage patterns on top and bottom surface of composite panels after piercing by abrasive water-jet	160
Figure 6.2	Comparison of (a) experimental and (b) simulated piecing process of the hybrid composite laminate	163
Figure 6.3	The progress of cutting sequence of the abrasive water-jet particles (white region) through the hybrid composite laminates at each step increment	165
Figure 6.4	Hole piercing with AWJ: Shear-out damage mechanism occurred on both and top and bottom side of the composite and significant internal delamination around the impact point	167

LIST OF ABBREVIATIONS

FRP	Fibre-Reinforced Polymer
AWJM	Abrasive Water-Jet Machining
DOE	Design of Experiment
RSM	Responses Surface Methodology
ANOVA	Analysis of Variance
SPH	Smoothed Particle Hydrodynamic
FEA	Finite Element Analysis
CMC	Ceramic Matrix Composites
MMC	Metal Matrix Composites
PMC	Polymer Matrix Composites
ROM	Rule of Mixture
LBM	Laser Beam Machining
EDM	Electric Discharge Machining
CNC	Computer Numerical Control
MRR	Material Removal Rate
HAZ	Heat Affected Zone
SOD	Stand Off Distance
CFD	Computational Fluid Dynamic
CA	Cellular Automata
WJ	Water-Jet
ALE	Arbitrary Lagrangian Eulerian
VARTM	Vacuum Assisted Resin Transfer Molding
RTM	Resin Transfer Moulding
ASTM	American Society for Testing and Materials
UTM	Universal Testing Machining
SEM	Scanning Electron Microscopy

EDX	Energy Dispersive X-ray
FCD	Face-Centred Composite Design
CMM	Coordinate Measuring Machine
PI	Prediction Internal
VUMAT	User-Defined Material Behaviour Subroutine

©This item is protected by original copyright

LIST OF SYMBOLS

P_h	Hydraulic Pressure
R_a	Average Arithmetic Surface Roughness
\dot{m}_A	Abrasive Flow Rate
V_f	Traverse Rate
M_i	Initial Mass of Specimen
M_{cr}	Remain Mass of the Fibre Reinforcement
M_f	Final Mass of Specimen
V_r	Volume Fraction of Specimen
R	Rate of Crosshead Motion
Z	Rate of Straining of Outer Fibre
L	Support Span of Specimen
d	Depth of Beam
T_R	Kerf Ratio
W_t	Top Kerf Width
W_b	Bottom Kerf Width
F_d	Delamination Factor
W_{max}	Maximum Width of Delamination area
W	Actual Width of Cut
R^2	Coefficient of Determination
V_A	Abrasive Velocity
ρ_w	Water Density
Ω	Domain
m^B	Mass of particle B
ρ^B	Density of particle B
F_{fib}^T	Tensile loads fibre damage

F_{fib}^C	Compressive loads fibre damage
ε_{11}^{OT}	Failure initiation for tension
ε_{11}^{OC}	Failure initiation for compression
E_{11}	Longitudinal elastic modulus
d_{fib}	Damage parameter of fibre
d_{11}^T	Tensile fibre-dominated damage parameter
ε_{11}	Current strain
ε_{11}^{FT}	Tensile failure strain
χ^T	Longitudinal tensile strengths
l_{fib}	Corresponding characteristic length

©This item is protected by original copyright

Prestasi Mekanikal dan Kebolehmesinan Komposit Polimer Bertetulang Gentian Hibrid dengan Menggunakan Pemesinan Jet Air-Bahan Lelas dengan Kaedah Permukaan Sambutan dan Model Berangka

ABSTRAK

Atas dorongan ke atas keperluan peralatan dan komponen yang menggunakan bahan lebih ringan dan kuat di dalam sektor penerbangan dan automotif, aktiviti penyelidikan untuk mencapai keperluan ini telah membangun dengan pesat. Kajian di dalam tesis ini adalah satu penyiasatan eksperimen mengenai pemotongan komposit polimer bertetulang gentian hibrid (FRP) dengan menggunakan pemesinan jet air-bahan lelas (AWJM). Sebelum proses pemesinan ini dijalankan, bahan rencam polimer bertetulang gentian hibrid dihasilkan di dalam pelbagai bentuk atau susunan rekaan menggunakan pemindahan damar pengacuan-vakum bagi tujuan penyaringan. Sifat mekanikal seperti kekuatan tegangan, kekuatan lenturan dan pecahan isipadu komposit hibrid ditentukan mengikut piawaian ASTM. Hasil penyaringan menunjukkan bahawa susunan [CW₂]₆ lebih unggul dari segi sifat mekanik, di mana C dan W adalah merupakan gentian karbon dan gentian kaca. Berdasarkan prestasi mekanikalnya yang cemerlang, keboleh-mesinan bahan rencam polimer bertetulang gentian hibrid [CW₂]₆ ini kemudiannya dikaji dengan lebih lanjut. Walaubagaimanapun, diketahui bahawa pemesinan bahan rencam FRP tanpa sebarang kerosakan adalah amat mencabar apabila menggunakan proses pemesinan konvensional. Hal ini disebabkan sifat tidak isotropik, keheterogenan, kepekaan termal, dan sangat lelas bahan rencam tersebut. Kajian secara komprehensif untuk menilai keberkesanan dan kombinasi parameter optimum pemesinan AWJ dengan nisbah *kerf*, kekasaran permukaan dan *delamination* (lapisan permukaan dan bawah) pada bahan rencam ini telah dijalankan dengan kaedah permukaan sambutan dan analisis varians. Reka bentuk faktorial 2^k yang mengikuti reka bentuk komposit berpusat (FCD) dengan sejumlah 30 eksperimen (16 titik faktorial-2⁴, lapan mata paksi-2⁴, dan enam mata pusat) digeriskan menggunakan perisian *Design Expert*. Hasil kajian dengan jelas telah menunjukkan bahawa pemotongan komposit ini adalah amat mencabar kerana penghasilan tirus *kerf* yang buruk, permukaan kasar dan *delamination* teruk di bahagian atas dan bawah permukaan yang dipotong. Keputusan analisa juga menunjukkan nisbah *kerf* dipengaruhi oleh jarak *stand-off* dan kadar terabas. Selain itu, kedua-dua bahagian *delamination* dipengaruhi oleh kadar aliran bahan lelas, kadar terabas, dan tekanan hidraulik. Kualiti permukaan terjejas oleh kadar aliran bahan lelas, jarak *stand-off*, kadar terabas dan tekanan hidraulik. Kesimpulannya, dengan meningkatkan tenaga kinetik aliran jet-air bahan lelas (pada kelajuan yang rendah) dapat mengurangkan nisbah *kerf*, kekasaran permukaan dan *delamination*. Penentuan parameter proses optimum dalam mencapai komposit berkualiti tinggi selepas proses pemesinan berada pada kadar aliran kasar 600 g/min, tekanan hidraulic 262.6 MPa, Jarak pendirian 2 mm dan kelajuan rendah melepasi 1000 mm/min. Dengan demikian, penyelidikan selanjutnya adalah untuk memahami mekanisme kerosakan permukaan di dalam keadaan laju tinggi AWJM melalui kaedah unsur terhingga serta zarah hidrodinamik lancar. Keputusan menunjukkan bahawa genangan zarah bahan lelas di titik impak menghasilkan retakan dan perambatan *delamination* dan seterusnya mekanisme ricihan. Persetujuan yang baik antara simulasi dan hasil eksperimen dari segi kualitatif dan kuantitatif telah dibuktikan melalui kajian khusus ini.

Mechanical Performance and Machinability of Hybrid FRP Composite Via Abrasive Water-Jet Machining using Response Surface Methodology and Numerical Model

ABSTRACT

Driven by the need for light-weight and high-strength materials for parts and components in the aviation and automotive sectors, research activities in attaining these requirements have been exponentially increased. This research describes an experimental investigation on the machinability of hybrid fibre reinforcement polymer (FRP) composites under abrasive water-jet machining (AWJM). Prior to machining, hybrid FRP composites of different architectures or arrangements were initially fabricated using resin transfer moulding for screening purposes. Mechanical properties such as tensile strength, flexural strength and volume fraction of the hybrid composites were determined per ASTM standards. Material screening experimentation indicates that the $[CW_2]_6$ arrangement, where C and W are weaved carbon fibre and glass fibre respectively, were superior in terms of mechanical properties. The machinability of $[CW_2]_6$ hybrid composites was then further investigated due to their excellent mechanical performance. However, it is well known that machining of FRP composites without any defect is extremely challenging when using conventional machining processes. This is mainly due to their inherent anisotropic, heterogeneous, thermal sensitivity, and highly abrasive of nature of fibre reinforcements. This research attempted to comprehensively evaluate the significant and optimal combination of AWJ machining parameters with respect to the kerf ratio, surface roughness and delamination (entrance and exit) on the hybrid FRP composite by the response surface methodology and statistical analysis of variance. A 2^k factorial design that follows a face-centred composite design (FCD) with a total of 30 experimental runs (16 factorial points— 2^4 , eight axial points— 2×4 , and six centre points) were outlined using Design Expert software. It is worth to note here that previous attempts in the trimming of composites has been challenging due to the presence of poor kerf taper, rough surface and severe delamination on top and bottom surface of trimmed surface. Experimental results revealed that the kerf ratio was influenced by the stand-off distance and traverse rate. On the other hand, both side of delamination were only influenced by abrasive flow rate, traverse rate, and hydraulic pressure. Lastly, surface quality was highly affected by the abrasive flow rate, stand-off distance, and traverse rate rather than the hydraulic pressure. In short, minimum kerf ratio, surface roughness, and delamination can be achieved by increasing the kinetic energy of abrasive water-jet stream when impinging into the composite under a lower speed. The optimum process parameters setting in achieving high-quality composites after the machining process were at abrasive flow rate of 600 g/min, hydraulic pressure of 262.6 MPa, stand-off distance of 2 mm and low traverse speed of 1000 mm/min. Further work on understanding the mechanism of surface damage under high velocity condition of AWJM has been developed using finite element method coupled with smooth-particle hydrodynamics. Results of this numerical model indicated that stagnation of abrasive particles at impact point generated delamination (crack initiation and propagation) and subsequently shear-out mechanisms. A good agreement was evident (qualitatively and quantitatively) between the simulation and experimental results in this particular study.

CHAPTER 1 : INTRODUCTION

1.1 Background

Hybrid fibre-reinforced polymer composites are extensively and exclusively developed in recent years through combination of two different fibre types in several distinct configurations. As depicted in Figure 1.1, hybrid fibre reinforced composites can be classified into interply, intraply, intimately mixed hybrid, and other configuration types (Kretsis, 1987; Zhang et al., 2012). Each configuration has its own unique advantages that relatively depend upon composite design structures and load expectations. Interply or intraply configurations are often designed to compose of low and high elongation fibres of different types. As claimed by Dong et al. (2013) and Swolfs et al.(2014), the primary purpose of hybridising these fibres is to synergising the superiority and moderating the shortcomings of individual fibres.

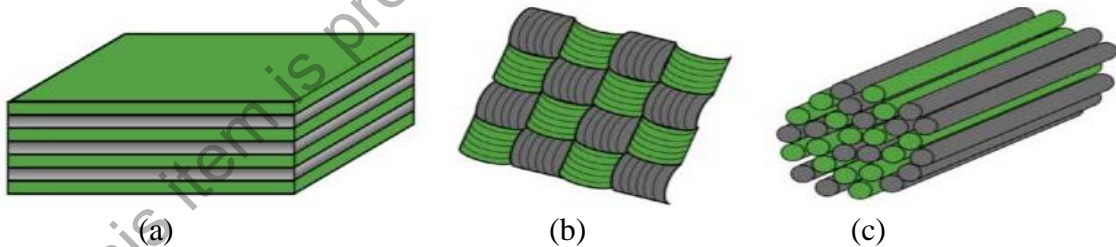


Figure 1.1 Hybrid composite configurations: (a) interply, (b) intraply, and (c) intimately mixed (Swolfs et al., 2014)

Fabrication of non-hybrid and hybrid fibre-reinforced polymer composites (FRP) typically involves combining, compacting, and processing the reinforcing fibres with polymer matrices. The fabrication processes or steps can be rather time-consuming and care intensive, which results in a substantial processing cost. Thus, they are typically produced to near-net shapes, through one of the following processes; namely, wet hand

lay-up, resin transfer moulding, and autoclave manufacturing. Despite the near-net shape process, final finishing processes which involve machining and cutting operations are essential to achieve any intricate shape requirements, critical part dimensions, and other functional needs, so that their subsequent manufacturing applications can be met. These applications include military equipment, aerospace component (e.g. wings, fuselages and tails), automotive transportation (e.g. luxury car bodies), sporting goods (e.g. badminton rackets and bicycle frames), and various other industrial applications.

Over the years, fundamental experimental studies on mechanical performance of carbon or glass FRP composites have attracted a significant attention of researchers worldwide. The primary interest of the research is to develop composites with improved performance to be qualified for the use in a broad spectrum of applications, particularly for high-performance aerospace and automotive components. However, the primary drawback of typical carbon fibre composites is their low compressive-to-tensile strength ratio, which can hinder mechanical performance (Dong et al., 2013). Likewise, glass fibre composites lack of high modulus-to-weight ratio property. In light of these drawbacks, hybrid FRP composites are developed to maintain superiority and overcome the moderate shortcomings of individual fibre types.

As aforementioned, the finishing processes through machining operations remain essential and are governed by a few important requirements. These include meeting tight dimensional, shape, and functional requirements. Trimming or machining operations are typically encountered during the early or first stage of manufacturing plan to bring the FRP composites into their desired and final form prior to assembly. Therefore, high quality and reliability requirements of FRP composites are of ultimate importance. This is due to the high cost of rework processes and discarding of damaged pieces. In addition,